FIELD EMISSION

Field emission of electrons into vacuum provides opportunities in areas currently addressed by traditional vacuum electronics and solid state devices, in addition to enabling a new class of devices (1). In addition to the replacement of the cathode ray tube by flat panel displays, the instant-on capability of unheated electron beam sources provides new instrumentation possibilities, and the ability to directly modulate emitted current densities at microwave frequencies will provide high-efficiency radio-frequency (RF) power in a compact package. These new technologies are made possible by recent advances in fabrication techniques and an improved theoretical understanding of field emission materials and structures. We first describe the process of field emission.

In the free-electron theory developed by W. Pauli and A. Sommerfeld, a metal is modeled as weakly bound valence electrons floating in a lattice of nuclei with their tightly bound electrons. In the interior of the metal, the electrostatic binding energy confines these "free" electrons within a potential well of depth ϵ_L. The energy states are fully occupied at two per level with the maximum denoted as the Fermi energy, ϵ_F. The additional energy required to extract an electron from the Fermi level into the vacuum is called the *work function,* ϕ. In a one-dimensional potential model, the metal–vacuum interface is characterized as a step of height $\epsilon_F + \phi$, as shown in Fig. 1.

Temperature effects modify the 0 K limit picture above as "hot" electrons occupy energy states greater than the Fermi level. When $kT \approx \epsilon_L - \epsilon_F$ some of the free electrons will escape over the wall of the potential well, a process referred to as *thermionic emission.* Other processes can elevate free electron energies in the vicinity of the metal–vacuum interface, such as in photoemission, in which the capture of energy quanta from light illuminating the surface allows electron emission.

When an electric field, F, is applied normal to the metal surface, an electron of energy ϵ directed normal to the surface sees a barrier to escape of height $\phi + \epsilon_F - \epsilon$ and of thickness $(\phi + \epsilon_F - \epsilon)/eF$.) For a low, narrow barrier, the electron may escape through it by the quantum mechanical process of tunneling. The quantum formulation of the electron wave function indicates a finite probability of barrier penetration due to uncertainty of the electron momentum, Δp. The Heisenberg uncertainty principle quantifies this as $\Delta p\ \Delta x \approx \hbar/2$, where $\hbar$ is Planck's constant divided by 2π. Electrons near the Fermi level encounter a barrier width of thickness ϕ/eF. This barrier height would classically require an additional electron momentum $\Delta p = (2\mathrm{m}\phi)^{1/2}$ for escape. The uncertainty principle $\Delta x \approx \hbar/2(2\mathrm{m}\phi)^{1/2}$. When this is on the order of the barrier width, $F[\mathrm{V/Å}] \approx 1.0(\phi\,[\mathrm{eV}])^{3/2}$ and electrons can "tunnel" through the barrier.

Transport through one-dimensional energy barriers may be approximated by the Wentzel–Kramers–Brillouin (WKB) method (2). Application of this method in a more accurate procedure allows a determination of current density to be anticipated for a given work function and applied electric field. This is the basis for the Fowler–Nordheim equation for emitted current density (3), $J[\mathrm{A/m^2}] = aF^2 \exp(-b\phi^{3/2}/F)$, with a and b constants which depend on work function. Since metals typically have work functions on the order of 3 eV to 5 eV, current densities of 10^6 A/m^2 to 10^7 A/m^2 over the emitting area are expected for the typically applied electric field magnitudes on the order of 0.5 V/Å.

Under the approximation that the tip field is proportional to the gate voltage and that the total emitted current is proportional to the current density, the form of the Fowler Nordheim equation suggests that $I(V_g) = A_{FN}\, V_g^2 \exp(-B_{FN}/V_g)$. Figure 2 shows typical experimental data (after Ref. 4), plotted on axes of $1/V_g$ and $\ln(I/V_g^2)$, for which a linear dependence is

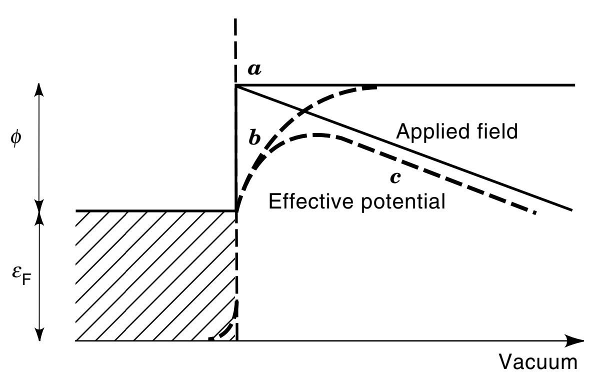

Figure 1. Energy band diagram for metal field emitter (a) zero degree limit, (b) image potential, (c) effect of applied electric field.

approximately obtained. Effects which cause a deviation from linearity are deferred to a later section.

Increased electron emission may be achieved by use of higher electric fields, lower work function materials, or combining current from multiple emitters. Since an electric field of 0.5 V/Å would require 5000 V to be applied over a distance of 1 μm for a parallel-plane capacitor geometry, alternative geometries and materials are desirable to reduce the applied voltage requirements. The spherical capacitor with distant outer conductor at potential = 0 has an electric field magnitude on the inner conductor, $F_{\text{sphere}} = V/r_{\text{sphere}}$. An electric field of 0.5 V/Å may be obtained with this geometry for an applied voltage of 25 V with a 50 Å radius—that is, on the order of currently available emitter tip radii. Geometrical enhancements have focused heavily on techniques for reduction of emitter tip radii consistent with other thermal, mechanical, and fabrication requirements.

The exponential term in the Fowler–Nordheim relation also contains the work function, ϕ which appears to the 3/2 power. Refractory metals have work functions in the 4 eV to 5 eV range. Low work function materials such as cesium ($\phi = 1.8$ eV) and barium ($\phi = 2.5$ eV) are chemically reactive and impose difficulties in the fabrication and operation environments. Reduced work function materials such as transition metal carbides have reduced work functions, $\phi \approx 3.5$ eV, which would increase current densities by roughly a factor of three over the refractory metals. Semiconductors such as silicon and diamond may also be used in the fabrication of field emitter devices. The energy band structure is more complicated; however, several advantages are anticipated. The extensive use of silicon in the solid-state device industry has generated an immense knowledge base in the processing and modification of the properties of silicon based materials. The compatibility inherent in use of silicon emitters integrated into the existing production stream is of great interest, as is the use of diamond for emitter fabrication due to the possibility of "negative electron affinity" to significantly reduce the effective work function of the emitting surface.

The use of field emitter arrays (FEAs) forms the basis for most of the vacuum microelectronic devices currently being

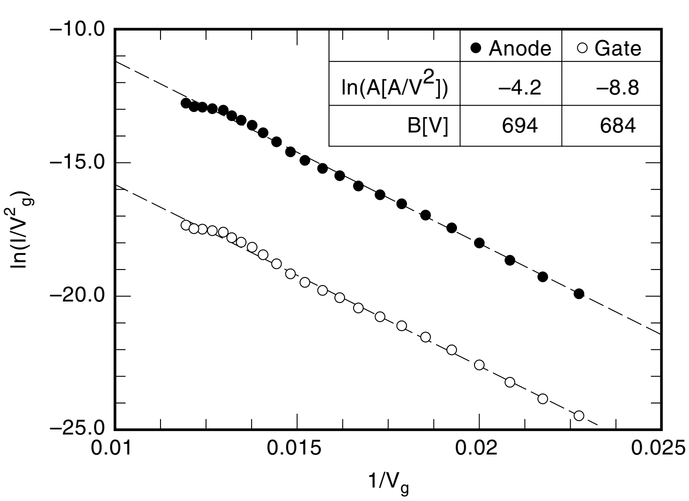

Figure 2. Fowler Nordheim representation of the current-voltage characteristics of an array showing the departure from linearity due to the influence of space charge.

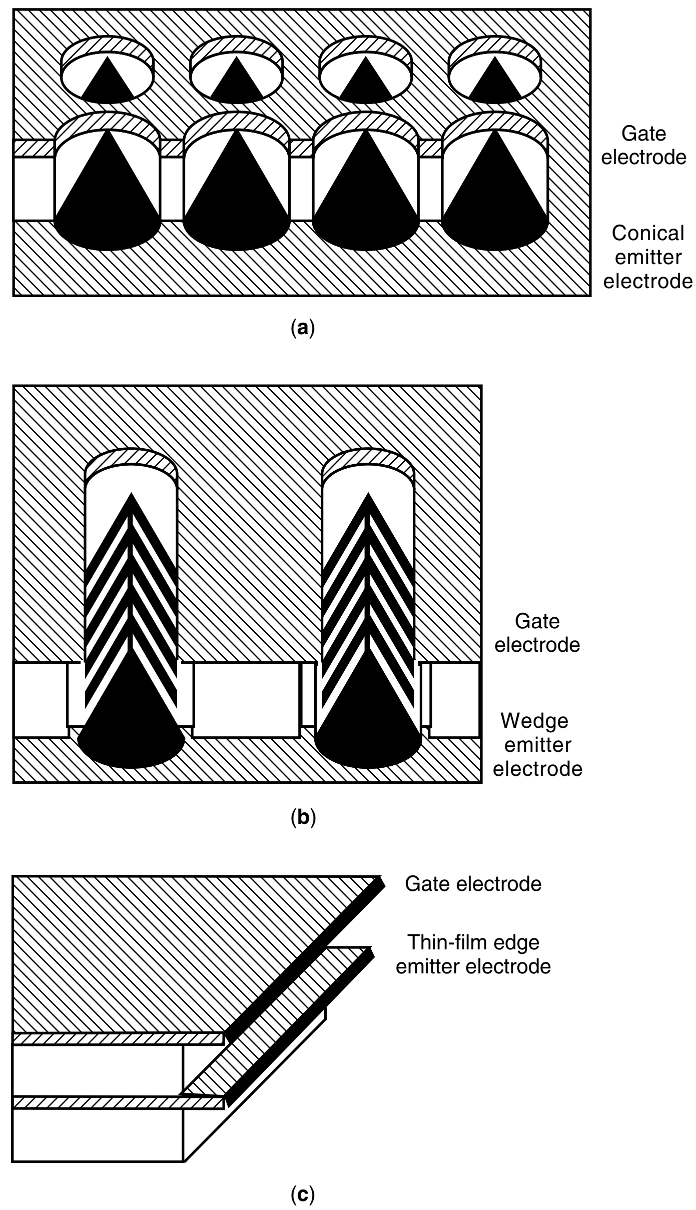

Figure 3. Field emitter array geometries: (a) Cone (Spindt), (b) wedge, (c) edge.

developed. The most prevalent geometry is that of the Spindt emitter (5). Within each unit cell, the emitter electrode is a cone whose apex is coplanar with a circular hole in a gate electrode plane, as in Fig. 3(a). The fabrication of field emitter structures is currently undergoing a transition from a stepper motor technology to the use of techniques such as interferometric lithography. A typical fabrication process (6) is characterized by four steps: (1) A silicon wafer is coated with a thin layer of chromium for an etch stop layer, up to 1 μm to 2 μm of silicon dioxide layer for an insulator layer, and a layer of tungsten or molybdenum for a gate electrode layer, followed by a mask layer of nickel. (2) The gate electrode metal and silicon dioxide layers are anisotropically etched, forming cylindrical holes. An additional etchback of the silicon dioxide undercuts the gate metal slightly. (3) A thin release layer (such as Al) is deposited followed by the evaporation of the

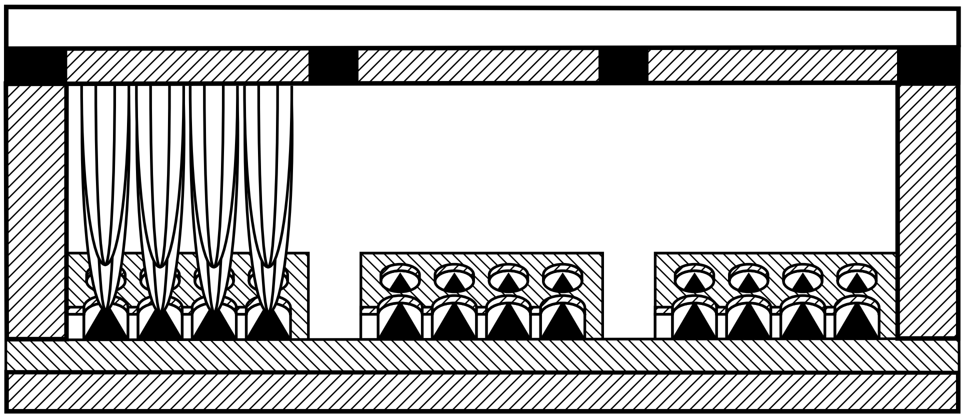

Figure 4. Field emitter display element schematic.

tip metal (often Mo). As evaporation progresses, the gate holes slowly close, decreasing the diameter of the metal deposition, and forming a conical shape. (4) The excess tip metal is removed over from the emitter cone and the gate electrode.

APPLICATIONS

Different devices place widely different demands on field emitters in terms of emission current density and modulation obtained with an imposed gate voltage. Lower development risk applications, such as flat panel displays, require relatively low current densities of 0.1 A/cm^2 and little or no modulation, whereas high-risk applications, such as emission gated microwave amplifiers, require greater than 100 A/cm^2, a frequency of modulation in the gigahertz range, and average to peak current ratios near 0.2.

Flat Panel Display

The use of field emitter electron sources in visual display systems range from a replacement for a conventional thermionic cathode in standard cathode ray tubes (CRT) to flat panel field emission displays (FED) with individually addressable emitter arrays for each pixel (7) as in Fig. 4. The higher currents, for the 30 kV X-ray limited anode voltage of the CRT, available from field emitters fitted within a given electron gun package allows higher brightness for the shorter pixel dwell time in high-definition television (HDTV). Flat panel field emission display (FED) applications, which are rapidly nearing volume production, are driven by several factors: image brightness and viewing angle, display size, pixel density and uniformity, power consumption, and cost. Engineering and manufacturing issues regarding reduced performance with low voltage phosphors versus the difficulty of anode positioning for high voltage use, emitter lifetime, compatibility with drive electronics, pixel uniformity, and device yield, are being addressed.

Already established flat panel technologies, such as active-matrix liquid crystal displays (AMLCD), are strong competitors to FEDs. Other display technologies, such as modifications to CRTs with its established knowledge base, plasma displays for high brightness wide view angle application, electroluminescent displays, vacuum fluorescent displays, passive LCD, and light emitting diodes, are less effective in addressing the broad market applicability. The significantly larger viewing angle, higher brightness, and lower power consumption anticipated for FEDs, coupled with predicted low costs, imply strong commercial market potential. In addition, the temperature tolerance and radiation resistance of FEDs indicate a strong potential for space and military applicability. Viewfinders, test and measurement equipment, electronic games, and night vision goggles are initial insertion candidates, followed by (as uniformity is increased) avionics displays and flat panel television.

FED manufacturers and design centers include: Pixel International, SA with a consortium including Raytheon; Futaba using molybdenum; Candescent Technology also using molybdenum; Samsung; Micron Display Technologies using silicon microtips; and SI Diamond Technology using diamond film emitters.

Instrumentation

The small dimensions of a typical field emission current source coincide with what is desired for diagnostic electron optics (see the article entitled ELECTRON MICROSCOPES. The exponential dependence of the emitted current upon the applied electric field, as seen in the Fowler–Nordheim equation, provides a sensitive technique which may be exploited in the development of new analytical instrumentation. Capacitive measuring devices may be constructed so that the emitted current is very sensitive to the anode distance for the given applied voltage. Atomic force microscopy uses this capacitance to float sharp tips over nanoscale structures. Relative position sensors and diaphragm vacuum gauges can be precise over an extended range of operation. Low pressures may be accurately measured by field-emitter-based ionization gauges where temperature and local perturbation due to outgassing variation is less of a problem than with thermionic filament Bayard–Alpert gauges yielding a wider range of accurate operation.

Micromachines

The application of micromachining techniques to fabricate structures at the micrometer scale and below has interesting synergy with field emission technology. Techniques developed for field emitters depend upon the construction of appropriate geometries in three-dimensional volumes. Moving structures are of prime importance in the creation of micromachines. The large electric forces generated at the emitter tips readily bend structures such as gate metalization. Potential uses include vibrators, motors, and capacitive displacement transducers.

Electron and Ion Beam Sources

Small size and emission stability is essential for applications such as electron holography (8). Many laboratory applications in surface analysis and ionization sources have emerged. The use of multibeam lithography could significantly enhance throughput of lithographic patterning with a massively parallel write capability. The highly efficient nature of field emission suggests the use of field emitters in space applications. These include active correction of spacecraft charging and use of spatially directed emission for propulsion.

Electronics for Demanding Environments

In addition to the hostile environment of space, where charged particle interception deteriorates solid-state electronics, nuclear reactors, and particle accelerators would benefit by use of radiation hard electronics. Temperature-insensitive electronics could become a new class of components for insertion into rockets, jets, auto engines, and fission power stations, to name a few. Higher-speed electronics due to reduction of electron transit time in vacuum-integrated circuits may be used for selected applications. The creation of devices based upon field emitter vacuum electronics provides robust solutions for these applications.

RF Amplifiers

Communications, electronic warfare, and radar are demanding applications that can benefit from higher current density and emission gating at gigahertz frequencies. In comparison to solid-state devices, field emitters may provide higher power operation with larger currents and a higher threshold for voltage breakdown, and also increased *band width* due to the higher electron mobility in a vacuum. Emission gating, rather than velocity modulation, may yield improved efficiency with a greatly reduced interaction length. Difficulties with using field emitters in these applications remain. The obstacles to straightforward implementations are (a) anode heating and (b) losses due to material resistivities with an attendant reduction in gain (9).

Two broad classes of devices have been identified, microdevices and macrodevices. Macrodevices use FEAs as cathode replacements while retaining a structural design similar to its traditional vacuum electronics counterpart. Microdevices are integrated into structures similar to solid-state counterparts. The typical unit cell is a microtriode or vacuum transistor wherein an anode is placed to collect the electrons produced by the gated FEA. These elements can also be distributed along a transmission line to increase gain and bandwidth. The linking of discrete FEA microtriodes by transmission lines to form a distributed amplifier was proposed by Koshmal (10). An integrated, continuous form of distributed amplifier was analyzed by Ganguly et al. (11).

A separation of the RF output circuit from the beam collection electrodes is used in the macrodevices currently being developed, which allows for increased power and/or bandwidth capability. The FEAs may be used simply as a cathode replacement, but, more importantly, bunching the electron beam at RF frequencies through emission gating may enable higher-efficiency operation. The output RF circuit may be of form similar to that used in traditional devices as shown in Fig. 5. A cavity output similar to klystrons is used to form an FEA-klystrode (12) [Fig. 5(a)], and a FEA-twystrode uses a traveling wave output circuit (13) [Fig. 5(b)]. Such devices are active areas of research (see VACUUM MICROELECTRONICS).

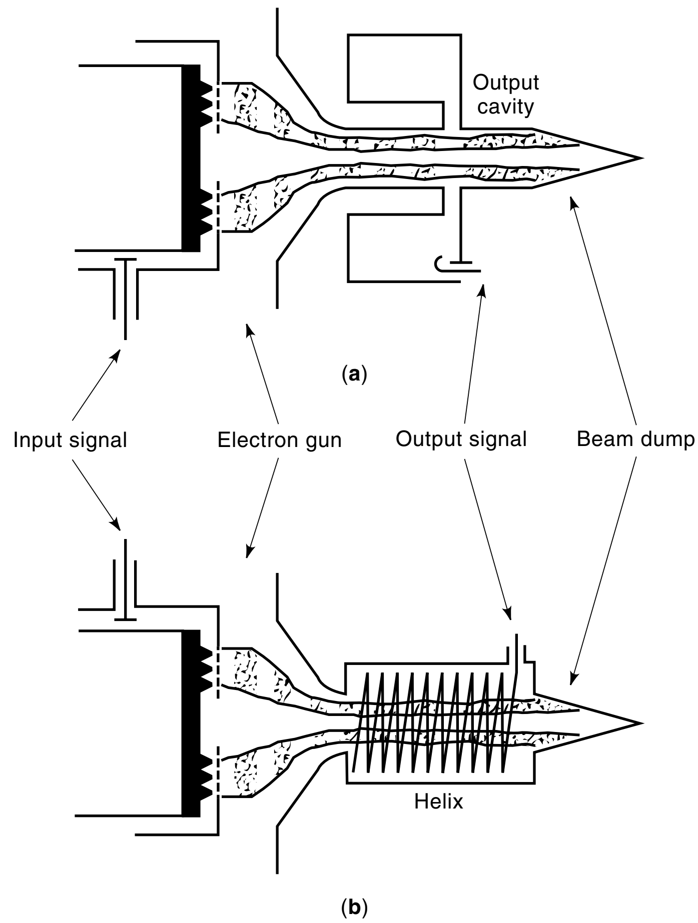

Figure 5. RF macrodevices. (a) klystrode, (b) twystrode.

ANALYSIS

A quantum mechanical theory of field emission must describe the electron source, the tunnelling barrier, and the resultant emitted current (14). The distribution of electrons near the surface may be described by a supply function. The characterization of the barrier which couples the bulk interior region to the exterior vacuum region is a complicated many-body problem of which the principal attributes are amenable to approximate techniques. The tunneling current is determined by integrating over momentum the product of the transmission probability, electron velocity, and supply function. The application of large electric fields, which is most readily done by sharpening of the emitter tip, strongly increases the emitted current. Diode and triode geometries determine the detailed distribution of the electric field on the emitter surface. The construction of practical devices requires consideration of materials and geometries in a design which addresses these processes. Field emission and tunneling quantities have atomic length and energy scales. Natural units to describe tunneling probabilities, work functions, and time scales are therefore atomic units (angstroms, electron volts, femtoseconds, and electron charge).

The Supply Function

The electron energies are given by the Fermi distribution $f(\epsilon_F, E) = 1/(1 + \exp(-(\epsilon_F - E)/\tau)$ at temperature τ/k_B giving an electron density by $n = \int f(\epsilon_F, E)\, dE$ (15). The Fermi level, ϵ_F, is related to the Fermi momentum (k_f) by $\epsilon_F = \hbar^2 k_f^2/2m$. Electron motion along the surface of a metal does not affect the estimation of the current, and so the transverse components of the Fermi momentum are integrated out, leaving a one-dimensional distribution, the supply function:

$$f_0(k) = \left(\frac{m}{\pi\tau\hbar^2}\right) \ln\left(1 + \exp(\alpha(k_f^2 - k^2))\right) \tag{1}$$

where $k_x \equiv k$ and $\alpha = \hbar^2\, \tau/2m$.

The Electron Effective Potential: Work Function, Fermi Level, and Image Charge

A description of electron motion in a bulk conductor is complicated owing to the strength of the Coulomb interactions between the particles and the large density of electrons in conductors, typically, $n \approx 10^{23}$ particles/cm^3 = 0.1 e/Å^3. The one-electron picture (16), useful for metals, describes the electron motion as governed by an effective local potential in which the metal ions are replaced by a uniform background of positive charge. The electron energy is then the sum of its kinetic energy and energies attributable to its interactions with the other electrons: Because electrons are fermions (Pauli exclusion principle), they will tend to be separated, giving rise to an "exchange energy"; similarly, the "correlation energy" accounts for the remaining many-body effects (17). Their sum is approximately given by (18,19)

$$\epsilon_{xc} = (13.6\text{ eV})\left(-\frac{0.916}{r} - \frac{0.88}{(r+7.8)}\right) \tag{2}$$

where the normalized radius r is related to the Bohr radius $a_0 = 0.529$ Å by $n - 1 = \frac{3}{4}\pi(ra_0)^3$.

At the metal and vacuum interface, the abrupt termination of the background positive charge plus the quantum mechanical penetration of the electron probability distribution into the vacuum creates a step in the one-electron potential as shown in Fig. 1. The work function, ϕ, is the energy required to remove one electron from the metal into the vacuum (19); it may be related to the electron density n by

$$\phi[\text{eV}] = \Delta\phi - \epsilon_F - \frac{d}{dn}\left(n\epsilon_{xc}(n)\right) \tag{3}$$

where discontinuity $\Delta\varphi = V(\infty) - V(-\infty)$, and $V(x)$ is evaluated by Poisson's equation from the electron density; $\Delta\varphi$ therefore includes a surface dipole term and the effects of a shift in the edge of the background positive charge to preserve global charge neutrality. The contribution of $\Delta\varphi$ can be approximated by treating the interior and exterior regions near the surface as a parallel plate capacitor of width L, for which $\Delta\varphi \approx 4\alpha\pi\hbar c L^2 n$. For metals such as molybdenum, taking r to be given by ($r \approx 2.922\ a_0$), then $n \approx 0.0646$ e/Å^3, $L \approx 0.3$ Å, $\epsilon_F \approx 5.87$ eV and consequently, Eq. (3) predicts $\phi \approx 2.1$ eV, which is comparable to the experimental range of 4.0 eV to 4.5 eV for molybdenum, the difference being due to the neglect of the ionic core potential contribution to the electron energy within the solid. An electron from the bulk impinging on the Mo surface therefore experiences a step-function potential of height $V_0 = \epsilon_F + \phi$. In the vacuum, the exchange and correlation potentials asymptotically match the classical image charge potential $V_i = -\alpha_{fs}\hbar c/4x \equiv Q/x$, where Q = 3.6 eV Å. It is standard practice in the one-electron potential to ignore the variations due to Friedel oscillations, due to the wave nature of the electron, within the metal ($V(x) = 0$) and to approximate the potential in vacuum by $V(x) = \epsilon_F + \phi - Fx - Q/x$, where F is the applied field, typically 0.3 to 0.7 eV/Å for field emission.

Tunneling Current, the WKB Approximation, and the Fowler–Nordheim Equation

Quantum mechanically, an electron impinging on a one-dimensional barrier has a finite probability of transmission even if its energy is below the barrier energy (2). The WKB method provides an analytical estimate of the tunneling probability (or the transmission coefficient $T(k)$) which is widely used in field emission studies (20) and which can be modified to treat semiconductors (21). The transmission coefficient rises exponentially with energy; because of the rapid decline of the supply function with energy, the transmitted electrons through the surface barrier ($T(k)f_0(k)$) are very narrowly peaked about the Fermi level. Consequently, the transmission coefficient may be approximated by $T_{wkb}(k) \approx \exp[-c_0 - c_1(k_f^2 - k^2)]$, where c_0 and c_1 depend on the work function ϕ and the applied field F.

The (one-dimensional) current through the barrier is given by integrating the product of the electron velocity with the number transmitted through the barrier

$$J(F) = \frac{1}{2\pi}\int_0^\infty \frac{\hbar k}{m} T(k) f_0(k)\, dk \tag{4}$$

For the image charge potential $V_i(x)$, the integral can be performed analytically (22), giving the current density $J(\epsilon_F, \phi, T, F)$, for which the Fowler–Nordheim equation (23) is a widely used limiting approximation, in which τ and ϵ_F tend to infinity:

$$J_{FN}(F, \phi) = a_{fn} F^2 \exp(-b_{fn}/F) \tag{5}$$

where $a_{fn} = (16\pi^2\hbar\phi t(y)^2)^{-1}$, $b_{fn} = 4\sqrt{(2m\phi^3)}\, v(y)/\tau\hbar F$. The quantities $t(y)$ and $v(y)$ are functions of elliptical integrals, and $y = \sqrt{(4QF)}/\phi$, and they may be approximated (23) by $t(y) \approx 1.057$ and $v(y) \approx 0.937 - 4QF/\phi^2$ with $Q = \alpha_{fs}\hbar c/4$.

Effects of Curvature on J_{FN}

In order to create the large fields necessary to get appreciable current, the conducting surface is sharpened in order to exploit field enhancement effects due to curvature. For example, the potential everywhere for a hemispherical conductor (boss) upon a plane is obtained from a Legendre polynomial expansion and results in (24,25)

$$V(r,\theta) = \phi + \epsilon_F - Fr\cos(\theta)\left(1 - \left(\frac{a_s}{r}\right)^3\right) - \frac{2Qa_s}{r^2 - a_s^2} \quad (6)$$

where a_s is the radius of the boss. The field is given by the negative gradient of the potential; along the symmetry axis of the boss, where $r = x + a_s$, the effects of curvature drop off quickly, allowing accurate expansion for small x. The Fowler–Nordheim equation form may be retained if the effective work function and tip field, $\phi_a \equiv \phi + Q/(2a_s)$ and $F_{tip} = 3F + Q/(4a_s^2)$, are used in Eq. (5). If the field F is due to a flat anode a distance D away, and neglecting the (typically small) term due to curvature, then $F_{tip} \approx 3V_{anode}/D$; the coefficient of V_{anode} is defined as the "field enhancement factor" (β) (and for a boss, it is independent of the boss radius). The introduction of curvature effects in this manner, while not entirely satisfactory as an approximation to three-dimensional tunneling effects (26) or as a representation of the atomically rough surface of an actual field emitter, does indicate the effect of tip curvature on the planar approximations.

Diode Geometry

Emitter surfaces are not spherical; rather, they are typically conical (e.g., "Spindt-type emitters") or wedges (e.g., "edge emitters") (27); when nonspherical geometries are considered, a_s refers to the local radius of curvature. For diode geometries with emitter and anode electrodes, analytical estimates of β, the field enhancement factors for hyperbolic wedges and cones (26,28,29,30) differ significantly. For a wedge, $\beta_{wedge} \approx 2/\pi\sqrt{a_s z_0}$, whereas for a cone, it is

$$\beta_{cone} = \frac{2}{a_s \ln\left(4\dfrac{z_0}{a_s}\right)} \quad (7)$$

where z_0 is the distance from emitter tip to anode plane and is equal to $a_s \cot^2(\theta_c)$, where θ_c is the wedge or cone half-angle of the emitter. Along the surface of the hyperbola, the field decreases according to $F(\rho) = F_{tip}/\sqrt{1 + (\rho/a_s \cos\theta_c)^2}$, where ρ is the radial distance from the axis of symmetry. In practice, edge emitters rely on surface roughness, in which microprotrusions analogous to bosses along the emitter edge give additional local field enhancement effects. This compensates (in combination with the larger emission area) for the lower fields produced for a given anode potential in the generation of total current compared to conical emitters.

Restricting attention to conical emitters (the treatment for wedge emitters is analogous), the total current for a given anode potential is obtained by integrating the one-dimensional Fowler–Nordheim current density over the emitter surface (25). The "area factor" b_{area} is the ratio of the total current $I(V_{anode})$ and the current density $J(F_{tip})b_{area} = I/J_{tip}$. For an emitter, represented by a hyperboloid of revolution,

$$b_{area} = 2\pi a_s^2 \cos^2\theta_c \left(\frac{F_{tip}}{b_{fn} + F_{tip}\sin^2\theta_c}\right) \quad (8)$$

where a_s is the radius of the emitter at the apex. a_s must be considered an effective radius, because microprotrusions, grain boundaries, and surface undulations (31) are present for real emitters. In simulations, a_s is taken to be on the order of 50 Å to 100 Å.

Triode Geometry

In the triode configuration, a nearby gate electrode creates the large electric fields at the apex of the emitter, and the anode collects the emitted current. In the case of a conical emitter, the gate hole diameter is of the same order as the emitter base diameter, and the gate is approximately coplanar with the emitter apex. The gate potential is typically orders of magnitude less than the anode potential in a diode configuration for comparable emitters, and the component of the field enhancement factor due to the anode (for the triode) is negligible unless collector-assisted emission is desired. In what follows, attention shall be restricted to the most common geometry of field emitter arrays, namely, the Spindt-type, or conical, emitter.

The simplest model of the triode, the "Saturn Model," replaces the anode by a uniform background field, the gate by a ring of charge, and the emitter by a sphere (25). The field enhancement factor so obtained is only qualitatively correct, but it suggests the manner in which Eq. (7) may be modified to account for the gate potential. Combining the Saturn and Diode models, the conical triode field enhancement factor is (32)

$$\beta_g \approx \left(\frac{\pi}{\ln\left(k\dfrac{a_g}{a_s}\right)} - \tan^2\theta_c\right)\frac{1}{a_s} \quad (9)$$

where the g subscript indicates that $F_{tip} = \beta_g V_{gate}$. The factor k depends on the geometrical details of the emitter and must be obtained by other means, such as analytical (33), Finite Difference (34), or Boundary Element methods (35); for a variety of unit cell dimensions, it may be approximated by $k \approx \frac{1}{54}(86 + a_s/a_s)\cot(\theta_a)$. By the use of Eq. (9) in the definition of tip field, the notion of area factor, as embodied in Eq. (8), may be retained in calculating total current from an individual gated field emitter.

COMPLICATIONS

A number of factors can cause departures from the emission characteristics described above. Imperfections in fabrication uniformity results in a distribution of emission across an array of emitters, altering the voltage dependence of the total current. In addition, the electric fields are modified by the presence of previously emitted electrons which reduce the measured currents to the anode. Limitations on device performance due to the present state of emitters and on application of field emitters due to the present state of device design must be examined to extend the range of applicability of field-emitter-based devices.

Statistical Variations

Measurements of arrays indicates nonuniformity of emission between individual emitters. This arises primarily from variation in emitter sharpness, but can also arise from work function changes caused by adsorbates and minor differences in geometry. The $I(V)$ relation of an individual emitter is, following Eq. (5), given by $I_i(V_g) = A_i\ V_g^2 \exp(-B_i/V_g)$, then a variation of tip radius will produce a distribution in B_i values for an array of conical emitters (36). The current for the array is then the statistical mean of the individual emitters multiplied by the N_{tips} and takes the Fowler–Nordheim-like form

$$I_{\text{array}}(V_{\text{gate}}) = A_{\text{FN}} V_{\text{gate}}^2 \exp(-B_{\text{FN}}/V_{\text{gate}}) \tag{10}$$

The value of B_{FN} depends primarily on the characteristics of the sharpest emitters, and then on the shape of the distribution. Choosing the linear distribution (30) $B_i = B_0 + \Delta(i-1)/(N_{\text{tips}}-1)$, where B_0 represents the sharpest emitter and Δ (measured in volts) denotes the spread in B values, is useful.

Using Eqs. (5), (8), and (9) for the emitters and letting $I_i(V_g) = \mathrm{b}_{\text{area}}(F_{\text{tip}})\ J_{\text{FN}}(F_{\text{tip}})$ and performing the sum over individual emitters results in analytical approximations for the "Fowler–Nordheim" A_{FN} and B_{FN} parameters (37)

$$\begin{aligned} B_{\text{FN}} &\approx \frac{b_{\text{fn}}}{\beta_g} + \frac{1}{x_0}(2+\lambda^2) \\ A_{\text{FN}} &\approx 2\pi a_s^2 \beta_g^3 \cos^2\theta_c a_{\text{fn}} \left(\frac{1-\exp(-x_0\Delta)}{x_0\Delta}\right) \frac{\exp\left(2+\frac{4}{3}\lambda^2\right)}{(b_{\text{fn}}x_0 + \beta_g \sin^2\theta_c)} \end{aligned} \tag{11}$$

where $x_0 = (V_{\max} + V_{\min})/2V_{\max}V_{\min}$, $\lambda = (V_{\max} - V_{\min})/V_{\max} + V_{\min})$, $V_{\max}$ is the largest gate voltage used, and $V_{\min}$ is the smallest and where λ and $x_0\Delta$ are assumed to be small quantities. One consequence of Eq. (11) is that as the voltage range over which $I(V)$ data is obtained increases, the B_{FN} value likewise increases, in accordance with experimentally observed behavior. The factor of 2 in the second term of B_{FN} and in the exponential of A_{FN} is due to two effects: One factor of unity is due to the hyperbolic geometry of an individual emitter, and the other factor of unity results from a statistical distribution of B values for an array of emitters.

Convexity in a Fowler–Nordheim Plot of $I_{\text{array}}(V)$: Distributions, Image Charge, and Space Charge

Competing effects give rise to changes in the linear relationship between $\ln(I(V)/V^2)$ vs $1/V$, as experimental data are usually represented. Positive, or concave up, convexity is due to a combination of a statistical distribution of emitters and the effect of variation of the surface electric field upon the current integrated over the emitter surfaces. Negative convexity, as seen in the high voltage regime in Fig. 2, is due to two sources: primarily, space-charge effects tend to suppress the field at the emitter tip, or, more importantly, tend to decrease the current reaching the collection anode by reflecting electrons back to the gate (37), as I_{array} is typically identified with I_{anode} (though in actuality, it is $I_{\text{anode}} + I_{\text{gate}}$); secondarily, deficiencies in the image charge potential used to calculate the one-dimensional $J(F)$ relations also introduce negative convexity (38), though the effect, by comparison to space charge, is small.

Space-charge effects (39) arise when the emitted current density from an array becomes so large that the presence of charge between the collection anode and the array suppresses the extraction field created by the anode. In a one-dimensional model, I_{array} exceeds I_{Child}, where the latter is the maximum current which may be transported across a planar diode configuration (40). Consequently, a virtual cloud of electrons forms above the gate plane, which can cause electrons to return to the gate; as such, space-charge effects are correlated with a rise in gate current. When electrons strike a conducting surface like the gate, gases desorb and (in the presence of the electron beam) become ionized, thereby potentially contributing to arc formation and array destruction.

DIRECTIONS FOR IMPROVEMENT

In addition to the difficulties associated with the individual emitter unit cell, the emitter performance is limited by both on-chip and off-chip constraints. The relatively large capacitance of the FEAs complicates the matching circuitry, particularly at RF frequencies. Different driver circuitry is needed for video applications, and on chip matching is required for demanding RF power applications.

Improvements in the design and construction of FEAs are necessary to increase device mean time before failure (MTBF). FEA failure mechanisms include thermal runaway, arcing, ion backbombardment, gate melting, and dielectric breakdown. Other sources for device failures appear due to additional adaptations and circuitry. The incorporation of FEAs into FEDs places strict requirements on large area yields and uniformity, necessitates the use of phosphors which will not poison the emitters, and stresses the need for cost-effective, rapid fabrication techniques.

As techniques addressing FEA uniformity and robustness are implemented, applications to instrumentation, micromachines, electron and ion beam sources, and electronics for demanding environments will appear. Problems are anticipated with the effects of ion backbombardment impacting and destroying the emission sites. The use of FEAs as cathodes in RF generation places severe constraints on device design to counter this through use of special materials, geometries, and improved vacuum.

Theoretical modeling of field emission processes will continue to examine alternate materials, coatings, and use of semiconductors. Studies including emission nonuniformity across the active areas on individual emitters and across arrays are required for improved noise performance and may provide new manufacturing metrics. Field emitter improvement will be sought in the areas of work function through coatings and surface modification, and in thermal robustness via structural adaptations.

Manufacturing techniques which emphasize scalability to large areas and fast fabrication are required for decreased cost. The timeliness and effectiveness of field emitter technology for commercial, scientific, and military uses will be seen in the near future.

BIBLIOGRAPHY

1. I. Brodie and P. Schwoebel, Vacuum microelectronic devices, *Proc. IEEE* **82**: 1006–1034, 1994.
2. E. Merzbacher, *Quantum Mechanics,* 2nd ed., New York: Wiley, 1994.
3. R. H. Fowler and L. W. Nordheim, Electron emission in intense fields, *Proc. R. Soc. London,* **A19**: 173, 1928; see also Ref. 20.
4. Data provided courtesy of R. A. Murphy (MIT-London Laboratory).

5. C. A. Spindt, A thin film field emission cathode, *J. Appl. Phys.,* **39**: 3504–3505, 1968.
6. C. Bozler et al., Arrays of gated field-emitter cones having 0.32 μm tip-to-tip spacing, *J. Vac. Sci. Technol. B,* **12** (2): 629–632, 1994.
7. FEDs: Wait a few years, *BYTE,* June 1995; also New LCD challenger to arrive around year 2000, *Future Watch, BYTE,* **22**(4): 28, April 1997.
8. A. Tonomura, Applications of electron holography, *Rev. Mod. Phys.,* **59**: 639–669, 1987.
9. J. P. Calame, H. F. Gray, and J. L. Shaw, Analysis and design of microwave amplifiers employing field-emitter arrays, *J. Appl. Phys.,* **73**: 1485–1504, 1993.
10. H. G. Kosmahl, A wide-bandwidth high-gain small-size distributed amplifier with field emission triode for the 10 to 3400 GHz frequency range, *IEEE Trans. Electron Devices,* **36**: 2728–2737, 1989.
11. A. K. Ganguly, H. Gray, and P. Phillips, Linear theory of a field-emitter-array distributed amplifier, *J. Appl. Phys.,* **67** (11): 7098–7109, 1990.
12. S. Bandy et al., Application of gated field emitter arrays in microwave amplifier tubes. *IEEE Conf. Rec. 1997 IEEE Int. Conf. Plasma Sci.,* 1997, p. 127.
13. M. A. Kodis et al., Operation and optimization of gated field emission arrays in inductive output amplifiers, *IEEE Trans. Plasma Sci.,* **24**: 970–981, 1996.
14. R. Gomer, *Field Emission and Field Ionization,* New York: American Institute of Physics, 1993.
15. R. Kubo, *Statistical Mechanics,* New York: North-Holland, 1965.
16. D. Pines, *The Many-Body Problem: A Lecture Note and Reprint Volume,* Reading, MA: Benjamin/Cummings, 1962, and articles reprinted therein.
17. J. Bardeen, Theory of the work function II. The surface double layer, *Phys. Rev.,* **49**: 653, 1939.
18. R. P. Feynman, *Statistical Mechanics: A Set of Lectures,* Reading, MA: Benjamin/Cummings, 1972.
19. N. D. Lang and W. Kohn, Theory of metal surfaces: Charge density and surface energy, *Phys. Rev.,* **B1**: 4555, 1970.
20. A. Modinos, *Field, Thermionic, and Secondary Electron Spectroscopy,* New York: Plenum Publ. Corp., 1984.
21. K. L. Jensen, Improved Fowler–Nordheim equation for field emission from semiconductors, *J. Vac. Sci. Tech.,* **B13**: 516, 1995.
22. K. L. Jensen and A. K. Ganguly, Numerical simulation of field-emission and tunneling—a comparison of the Wigner function and transmission coefficient approaches, *J. Appl. Phys.,* **73**: 4409, 1993.
23. C. A. Spindt et al., Approximating $t(y)$ as a constant and $v(y)$ as a quadratic was suggested, *J. Appl. Phys.,* **47**: 5248, 1976.
24. J. D. Jackson, *Classical Electrodynamics,* 2nd ed., New York: Wiley, 1975.
25. K. L. Jensen, E. G. Zaidman, and M. A. Kodis, Analytical and seminumerical models for gated field emitter arrays I & II, *J. Vac. Sci. Tech.,* **B14**: 1942, 1996.
26. P. H. Cutler et al., Tunneling theory and vacuum microelectronics. In R. Turner (ed.), *Vacuum Microelectronics 89,* Inst. Physics Conf. Series #99, Bristol, England, 1989 (and references therein); J. W. Gadzuk and E. W. Plummer, Field emission energy distribution (FEED), *Rev. Modern Phys.,* **45**: 487, 1973 and references therein.
27. Bo Lee et al., Knife-edge thin film field emission cathodes on (110) silicon wafers, *J. Vac. Sci. Technol.,* **B12**: 644, 1994; "Volcano" geometries can be considered edge emitters, in H. Busta et al., Volcano-shaped field emitters for large area displays, *Tech. Dig., Int. Electron Devices Meet.,* Washington, DC, 1995, 16.5.1.
28. G. Arfken, *Mathematical Methods for Physicists,* 3rd ed., Orlando, FL: Academic Press, 1985.
29. J. P. Barbour et al., *Phys. Rev.,* **92**: 45, 1953; W. P. Dyke, J. K. Trolan, E. E. Martin, J. P. Barbour, *Phys. Rev.,* **92**: 1043, 1953.
30. K. L. Jensen et al., NRL Tech. Memor. NRL/FR/6840-95-9782, 1995.
31. W. D. Goodhue et al., Bright Field analysis of field-emission cones using high-resolution transmission electron microscopy and the effect of structural properties on current stability, *J. Vac. Sci. Technol.,* **B12**: 693, 1994.
32. K. L. Jensen et al., Electron emission from a single spindt-type field emitter: Comparison of theory with experiment, *Appl. Surf. Sci.,* **111**: 204, 1997.
33. Luo Enze, Liu Yunpeng, and Huang Wenhu, A general formula to calculate the field intensity on the field emitter. In R. Turner (ed.), *Vacuum Microelectronics 89,* Inst. Physics Conf. Series #99, Bristol, England, 1989 (and references therein) for a review.
34. W. Dawson Kesling and Charles E. Hunt, Field emission device modeling for application to flat panel displays, *J. Vac. Sci. Technol.,* **B11**: 518, 1993; D. W. Jenkins, Emission area of a field emitter array, *IEEE Trans. Electron Devices TED,* **40**: 666, 1993; E. G. Zaidman, Simulation of field emission microtriodes, *IEEE Trans. Electron Devices,* **TED 40**: 1009–1016, 1993.
35. See, for example: A. Renau, F. H. Read, and J. N. H. Brunt, The charge-density method of solving electrostatic problems with and without the inclusion of space-charge, *J. Phys. E: Sci. Instrum.,* **15**: 347, 1982; R. L. Hartman, W. A. Mackie, and P. R. Davis, Use of boundary element methods in field emission computations, *J. Vac. Sci. Technol.,* **B12**: 754, 1994.
36. J. D. Levine, Statistical analysis of field emitter emissivity: Application to flat displays, *J. Vac. Sci. Technol.,* **B13**: 553, 1995.
37. K. L. Jensen, M. A. Kodis, R. A. Murphy, and E. G. Zaidman, Space Charge Effects on the current–voltage characteristics of gated field emitter arrays, *J. Appl. Phys.,* **82**: 845–854, 1997.
38. P. H. Cutler and D. Nagy, *Surf. Sci.,* **3**: 71, 1964; P. H. Cutler, J. He, N. M. Miskovsky, T. E. Sullivan, and B. Weiss, *J. Vac. Sci. Tech.,* **B11**: 387, 1993.
39. In addition to Ref. 37, see: J. P. Barbour et al., *Phys. Rev.,* **92**: 45, 1953; W. P. Dyke et al., *Phys. Rev.,* **92**: 1043, 1953; W. A. Anderson, Role of space charge in field emission cathodes, *J. Vac. Sci. Tech.,* **B11**: 383, 1993; G. N. A. van Veen, Space Charge effects in Spindt-type field emission cathodes, *J. Vac. Sci. Tech.,* **B12**: 655, 1994.
40. C. K. Birdsall and W. B. Bridges, *Electron Dynamics of Diode Regions,* New York: Academic Press, 1966.

ERNEST G. ZAIDMAN
Naval Research Laboratory
KEVIN L. JENSEN
Naval Research Laboratory

FIELD EMITTER ARRAYS (FEA).

See FIELD EMISSION.